T·H·E OHIO STATE UNIVERSITY

A DIAGNOSTIC TECHNIQUE USED TO OBTAIN

CROSS RANGE RADIATION CENTERS FROM ANTENNA PATTERNS

T.H. Lee
W.D. Burnside

The Ohio State University

ElectroScience Laboratory

Department of Electrical Engineering
Columbus, Ohio 43212

NOTICES

When Government drawings, specifications, or other data are used for any purpose other than in connection with a definitely related Government procurement operation, the United States Government thereby incurs no responsibility nor any obligation whatsoever, and the fact that the Government may have formulated, furnished, or in any way supplied the said drawings, specifications, or other data, is not to be regarded by implication or otherwise as in any manner licensing the holder or any other person or corporation, or conveying any rights or permission to manufacture, use, or sell any patented invention that may in any way be related thereto.

TABLE OF CONTENTS

LIST OF FIGURES

I. INTRODUCTION

Microwave imaging techniques have been widely used by the scattering community to identify the scattering centers associated with a complex target [1]. For example, a two-dimensional image is typically formed in the radial (down-range) and normal to the radial (cross-range) directions. The down-range scattering centers are normally determined by processing the backscattered fields from the object with a wide-band signal illuminating the object. The cross-range scattering centers can be determined by either Doppler processing or synthetic aperture processing the backscattered fields with a constant frequency signal illuminating the object. The two-dimensional image of a target such as shown in Figure 1 [1] indicates the scattering intensity level associated with various scattering centers of the target. This type of data is extremely useful for diagnostic purposes because one can evaluate the various scattering centers and their relative scattering levels. Then as changes are made on the structure one can quickly observe how a given scattering center is affected by the changes even though the change might be insignificant in terms of the total structural scattering level.

Microwave holographic techniques [2] have been used recently for the determination of amplitude and phase of the principal and cross-polarized aperture fields of large aperture antennas. Using that approach, the complex far-zone fields of the antenna in θ-ϕ directions, around the main beam, are processed via a Fourier Transform to obtain the aperture fields. From the aperture phase data, one can further
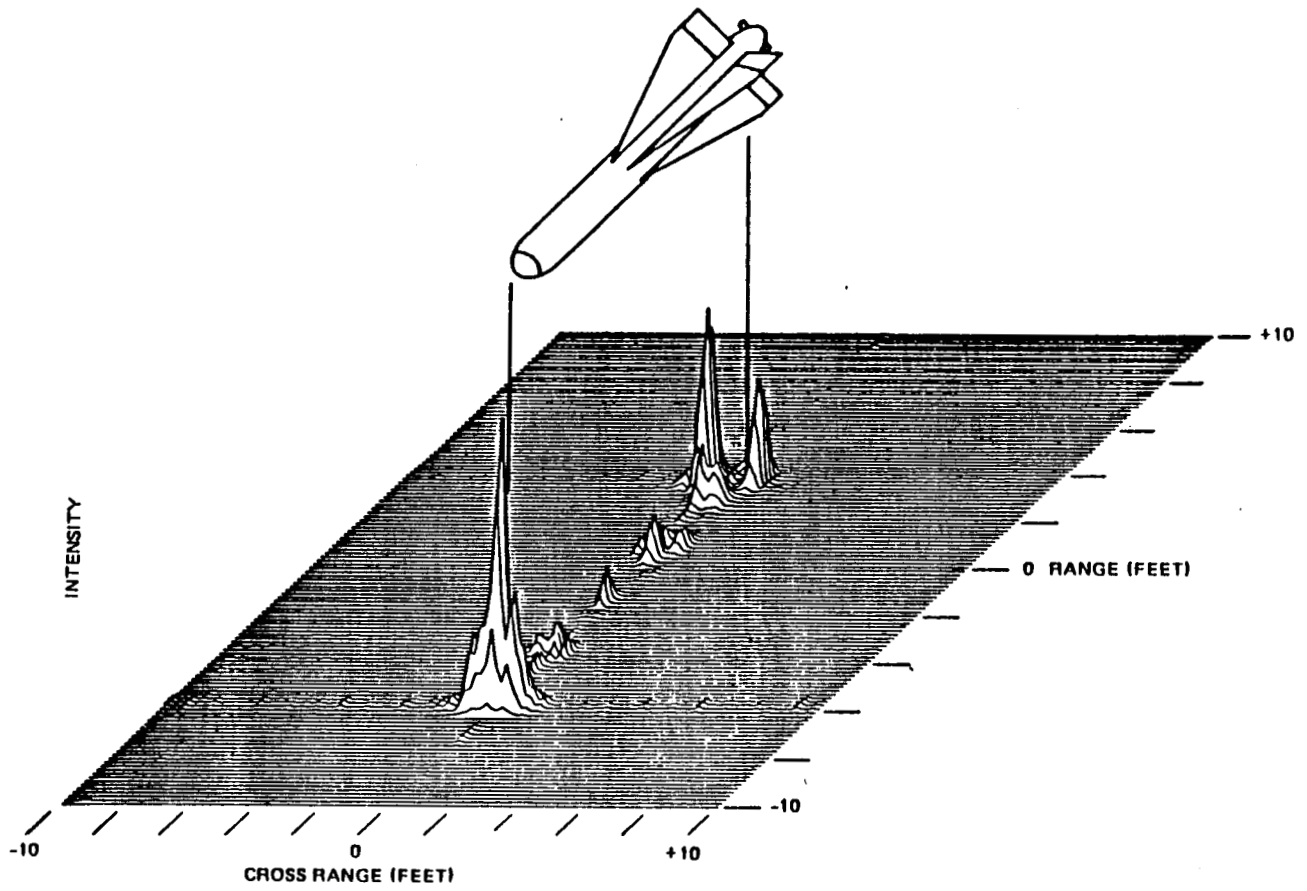
1

Figure 1.   Two-dimensional image of a missile body [1].

2

determine the possible antenna surface deviations relative to its ideal geometry [3]. Using a similar method, one can determine the locations of the various radiation centers which contribute to the far out sidelobes of an antenna pattern. This technique, which forms the basis of this report, utilizes the amplitude and phase of the antenna pattern to identify the appropriate centers. The formulation of this technique is given in the next section. Results of cross range processing the radiation patterns for two 8' reflector antennas, a prime focus fed and a Cassegrainian, are presented later.

II. FORMULATION

Let $P(\theta)$ be the radiation pattern of an antenna in a given ρ-z plane (constant ϕ) with its phase center at a coordinate origin, which is also the center of rotation, as shown in Figure 2(a). If the phase center of the antenna is moved to point A, as shown in Figure 2(a), the pattern of this same antenna is given by

$$P'(\theta) = P(\theta)e^{-jkR_d\cos(\theta_d-\theta)} \tag{1}$$

where R_d and θ_d define the new phase origin, A. Note that the e^{-jkr}/r factor has been suppressed from the antenna pattern. If Equation (1) is integrated over a small angular region around $\theta \approx \theta_0$; i.e., $\theta_0 - \Delta\theta \leq \theta \leq \theta_0 + \Delta\theta$, the following integral is obtained:

$$I' = \int_{\theta_0-\Delta\theta}^{\theta_0+\Delta\theta} P'(\theta)d\theta = \int_{\theta_0-\Delta\theta}^{\theta_0+\Delta\theta} P(\theta)e^{-jkR_d\cos(\theta_d-\theta)}d\theta . \tag{2}$$
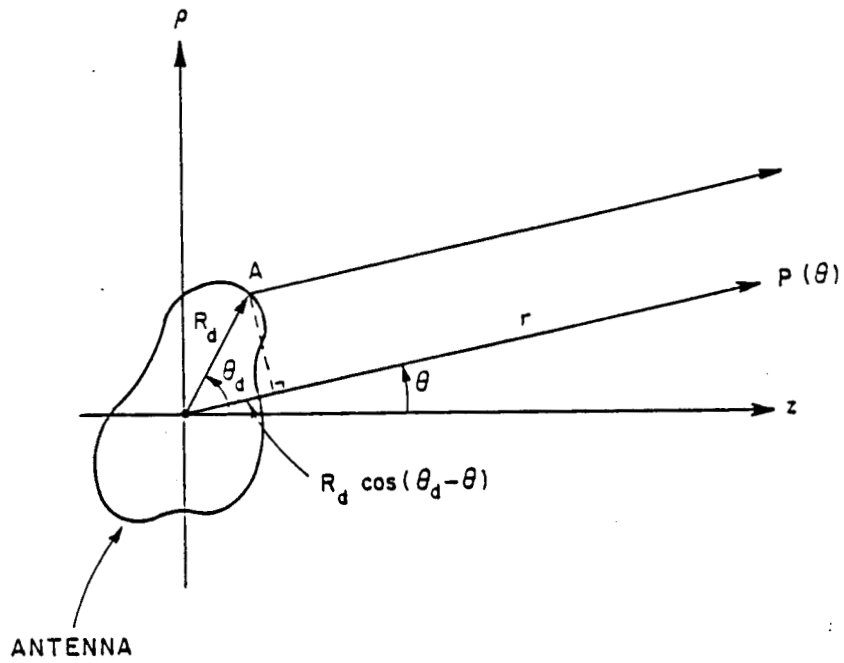
(a) Original geometry
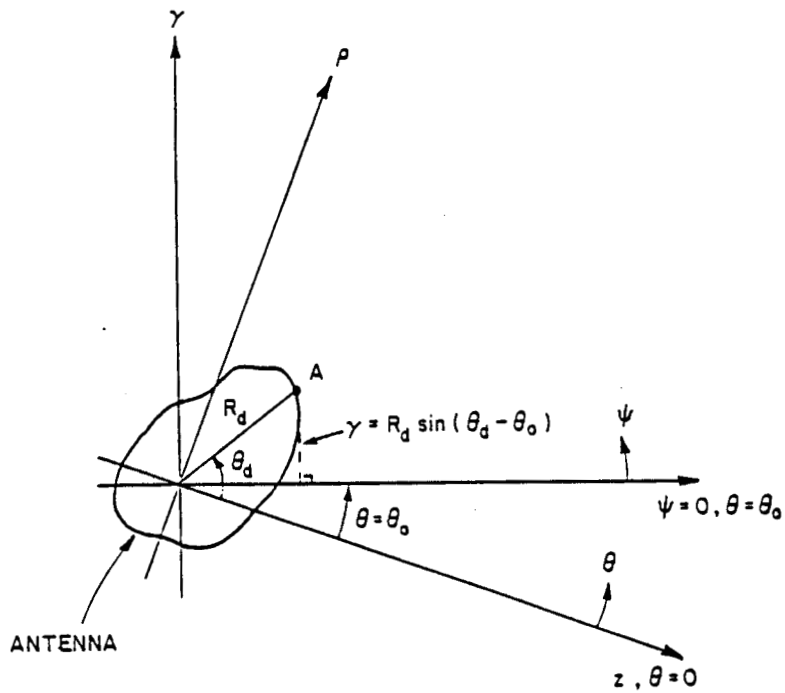
(b) Rotation of coordinate system, $\psi = \theta - \theta_o$

Figure 2. Geometry of an antenna on a given ρ-z plane (constant ϕ plane).

Let $\psi = \theta - \theta_o$, then Equation (2) becomes

$$I' = \int_{-\Delta\theta}^{\Delta\theta} P(\psi + \theta_o) e^{-jkR_d \cos(\theta_d - \theta_o - \psi)} \, d\psi \ . \tag{3}$$

The cosine term in the above integral can be written as

$$\cos(\theta_d - \theta_o - \psi) = \cos(\theta_d - \theta_o)\cos\psi + \sin(\theta_d - \theta_o)\sin\psi \ .$$

If it is assumed that ψ is small; i.e., $\Delta\theta$ is small since $-\Delta\theta \leq \psi \leq \Delta\theta$, then one obtains

$$\cos(\theta_d - \theta_o - \psi) \approx \cos(\theta_d - \theta_o) + \sin(\theta_d - \theta_o)\psi \tag{4}$$

Thus, Equation (3) becomes

$$I' = \int_{-\Delta\theta}^{\Delta\theta} P(\psi + \theta_o) e^{-jkR_d [\cos(\theta_d - \theta_o) + \sin(\theta_d - \theta_o)\psi]} \, d\psi$$

or

$$I' = e^{-jkR_d \cos(\theta_d - \theta_o)} \int_{-\Delta\theta}^{\Delta\theta} P(\psi + \theta_o) e^{-jkR_d \sin(\theta_d - \theta_o)\psi} \, d\psi \ . \tag{5}$$

The rotation in the coordinate system, $\psi = \theta - \theta_o$, is illustrated in Figure 2(b). By neglecting the constant phase term, Equation (5) can now be written in the following form:

$$I(\gamma) = \int_{-\Delta\theta}^{\Delta\theta} P(\psi + \theta_o) e^{-jk\gamma\psi} \, d\psi \tag{6}$$

5

where $\gamma = R_d \sin(\theta_d - \theta_o)$. By making γ an independent variable such that $\gamma_i \leq \gamma \leq \gamma_f$, one obtains a response function, $I(\gamma)$. It is shown next by using an isotropic point source that the response $I(\gamma)$ provides information about the location of the radiation center along the γ-axis; i.e., the cross range location of a source of radiation or radiation center. Note that the pattern function of the antenna, $P(\theta)$, is measured or calculated with respect to the coordinate origin.

The radiation pattern of an isotropic point source located at point A as shown in Figure 2(a) with its phase center at the coordinate origin is given by

$$P(\theta) = e^{jkR_d\cos(\theta_d - \theta)} .$$

From Equation (6), one obtains that

$$I(\gamma) = \int_{-\Delta\theta}^{\Delta\theta} P(\psi + \theta_o)e^{-jk\gamma\psi}d\psi = \int_{-\Delta\theta}^{\Delta\theta} e^{jkR_d\cos(\theta_d - \theta_o - \psi)}e^{-jk\gamma\psi}d\psi. \quad (7)$$

Note that γ is now an independent variable. By using the same approximation given in Equation (4) since ψ is small, Equation (7) becomes

$$I(\gamma) = \int_{-\Delta\theta}^{\Delta\theta} e^{jkR_d\cos(\theta_d - \theta_o)}e^{jk[R_d\sin(\theta_d - \theta_o) - \gamma]\psi}d\psi$$

or

$$I(\gamma) = e^{jkR_d\cos(\theta_d - \theta_o)} \frac{2\sin\{k[R_d\sin(\theta_d - \theta_o) - \gamma]\Delta\theta\}}{k[R_d\sin(\theta_d - \theta_o) - \gamma]} .$$

6

The magnitude of $I(\gamma)$ after normalization is given by

$$|I(\gamma)|_N = \left| \frac{\sin\left\{k[R_d\sin(\theta_d-\theta_o)-\gamma]\Delta\theta\right\}}{k[R_d\sin(\theta_d-\theta_o)-\gamma]\Delta\theta} \right| . \qquad (8)$$

It is apparent from Equation (8) that $|I(\gamma)|_N$ is a function of the form $\left|\frac{\sin u}{u}\right|$, which has a maximum at $u=0$. Consequently, the maximum of the response $I(\gamma)$ occurs at

$$\gamma = R_d\sin(\theta_d-\theta_o) \qquad (9)$$

which is exactly the position of the isotropic point source along the cross range axis; i.e., the γ-axis.

From this simple example, the interpretation of Equation (6) becomes clearer. If the radiation center is at $\gamma=\gamma_o$, the product of the pattern function $P(\psi+\theta_o)$ and the phase factor $e^{-jk\gamma_o\psi}$ for small ψ angles will be coherent. Consequently, the summation of these coherent integrands, $I(\gamma_o)$, provides a higher response than the responses for other γ's. This is the same idea as the synthetic aperture processing used for scattering problems.

If more than one radiation center is present, the integral given by Equation (6) can be used to find the cross range response and their positions provided that the adjacent centers are separated far enough so that their locations can be resolved. It is also noted that for different pattern angles, θ_o, one obtains different response functions, $I(\gamma)$, to determine where the radiation contributions to the pattern at

7

θ_o are coming from. In the next sections, the radiation patterns of an 8' prime focus fed reflector antenna and an 8' Cassegrain reflector system are used to illustrate the value of this cross range processing technique.

III. NUMERICAL RESULTS

A. 8' Prime Focus Fed Reflector

In this section, the results of cross range processing of the patterns of an 8' prime focus fed reflector are presented. The reflector had a 48" focal length and a feed support structure which includes a circular ring and four struts with a 0.84" diameter and 90° angular separation. The geometry of this reflector is illustrated in Figure 3(a). The measured far-zone H-plane pattern at 11.0 GHz with a corrugated horn feed is shown in Figure 3(b). The cross range responses based on the measured data and for $\theta_o=0°$, 20°, and 40° with $\Delta\theta=5°$ are shown in Figure 4. In order to determine the locations of the radiation centers, the reflector geometries and the projections of the struts are also shown in the same figure. Note that the center of rotation of the reflector was 21.5" from the vertex of the reflector. It is apparent from Figure 4(a) that the contributions to the radiated field at $\theta_o=0°$ are from the whole aperture of the reflector, as expected; although there are minor perturbations associated with the scattered fields from the feed support structure. From Figures 4(b) and 4(c), one can identify the radiation centers, which are two edge diffraction points, the end points of the struts attached to the reflector and the feed

8
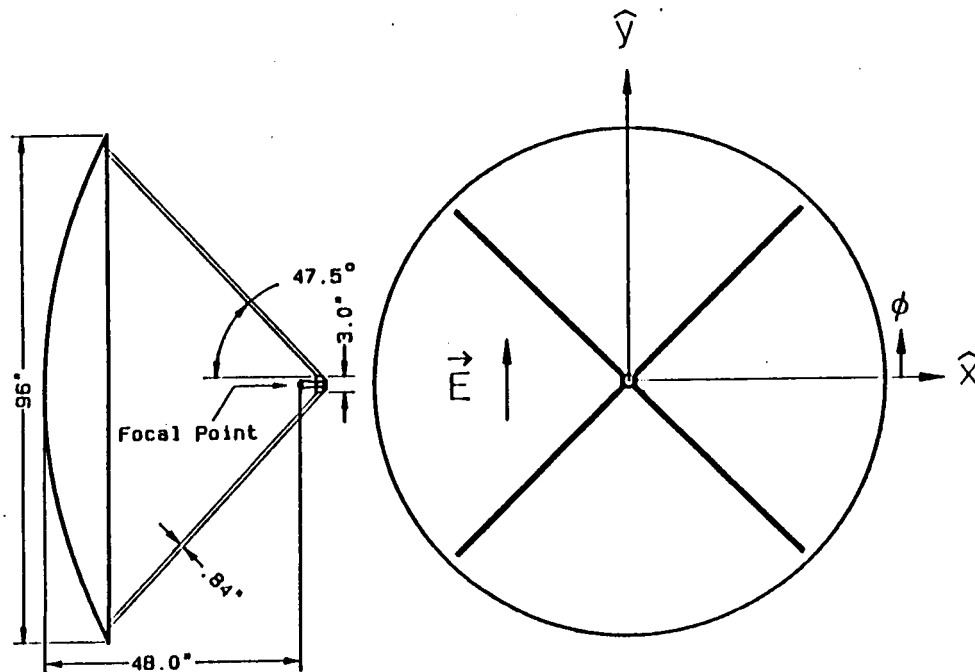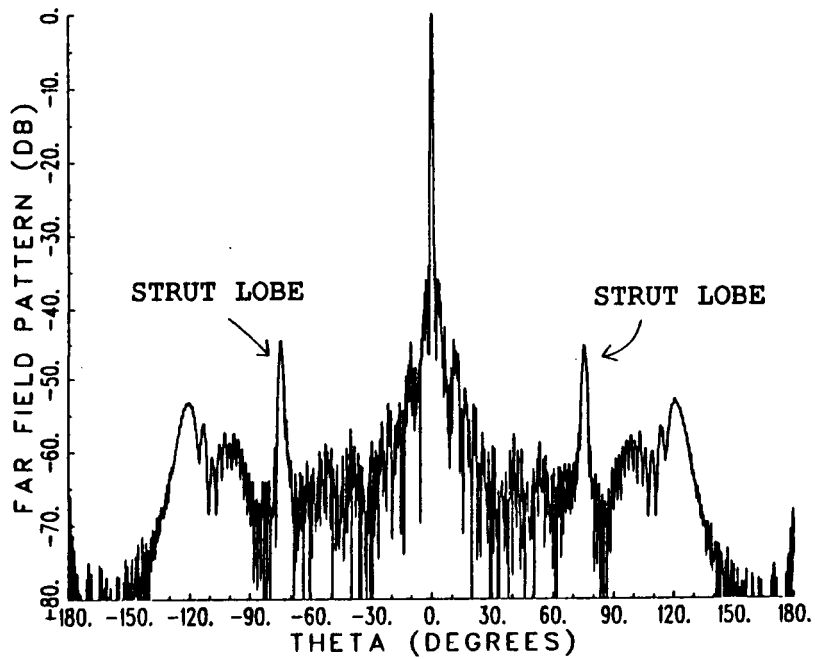
(a) Geometry

(b) Measured H-plane pattern

Figure 3.   Geometry and measured H-plane pattern of the 8′ prime focus
fed reflector.

9

(a) $\theta_o = 0°$, $\Delta\theta = 5°$

(A): MAIN REFLECTOR EDGE
(B): STRUT END POINT
(C): FEED SPILLOVER, SUPPORT STRUCTURE
(D): HOLE
(E): STRUT END POINT
(F): MAIN REFLECTOR EDGE
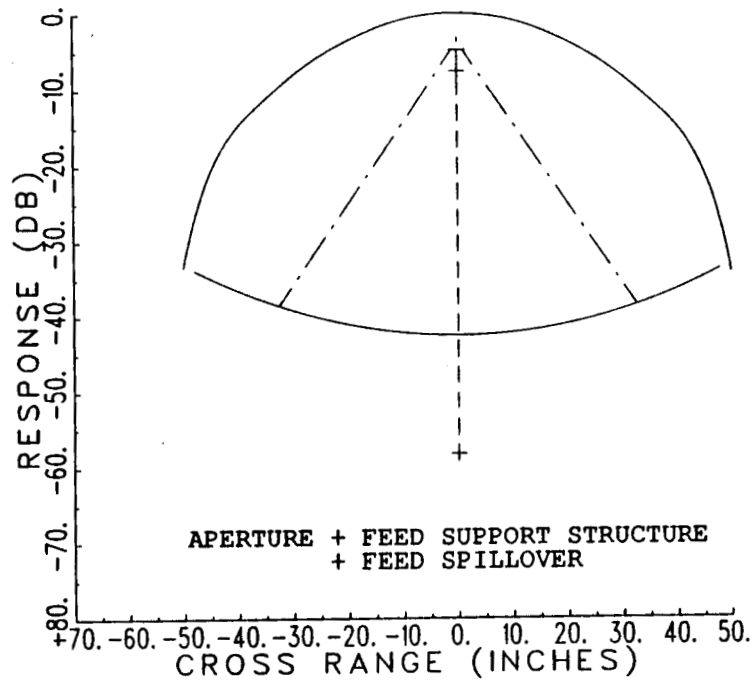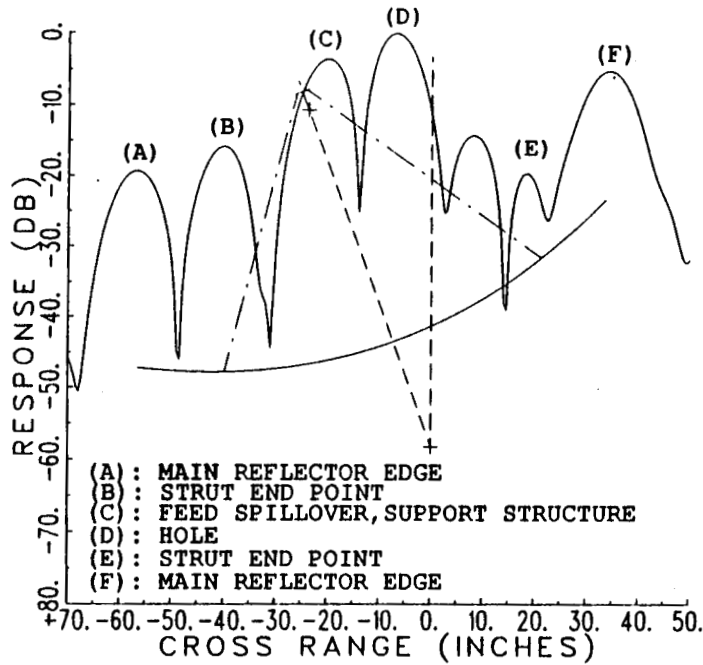
(b) $\theta_o = 20°$, $\Delta\theta = 5°$

Figure 4. Cross range response of the measured H-plane pattern for the 8' prime focus fed reflector.

(A): MAIN REFLECTOR EDGE
(B): FEED SPILLOVER,SUPPORT STRUCTURE,
     STRUT END POINTS
(C): HOLE
(D): MAIN REFLECTOR EDGE,STRUT END POINTS
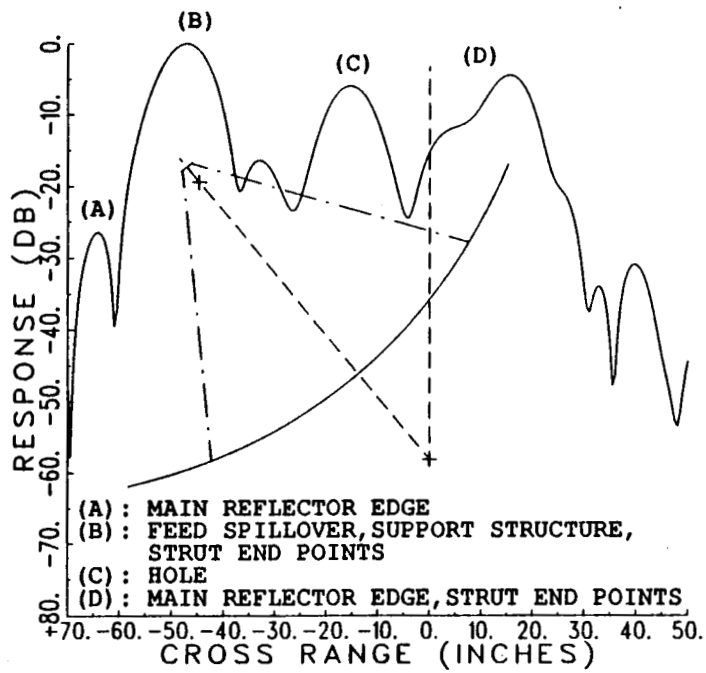
(c) $\theta_o=40°$, $\Delta\theta=5°$

Figure 4.   Continued.

11

support structure in the neighborhood of the focus. It is also seen from Figures 4(b) and 4(c) that there is a very strong response at $\gamma = -7.5"$ for $\theta_o = 20°$ and at $\gamma \approx -14.0"$ for $\theta_o = 40°$. This is due to a 2.5" diameter hole centered at the vertex of the reflector which was created during the m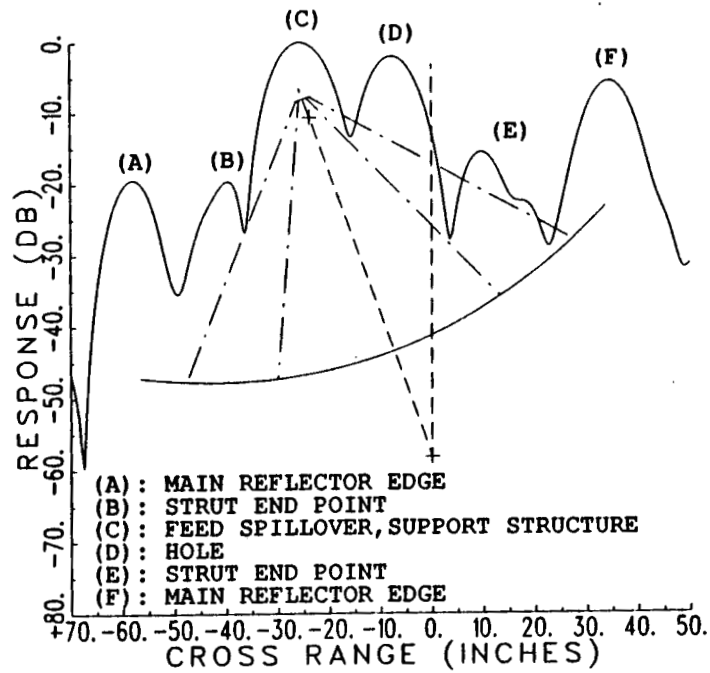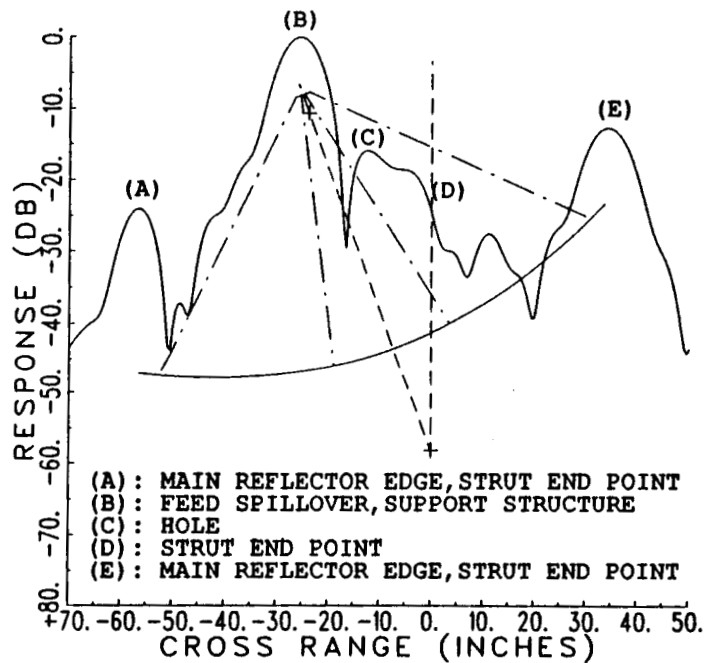anufacture process of the reflector. Although this hole was taped from behind the dish during the pattern measurement, the effects due to this hole and its discontinuity still shows up in the patterns. This fact is further verified by processing the measured off-principal plane patterns ($\phi = 15°$ and $30°$ cuts) at $\theta_o = 20°$ which are shown in Figure 5. Note that the cross range processing indicates a radiation center at the center of the reflector for each ϕ pattern cut which identifies the hole as a significant scattering center. This example illustrates the diagnostic value of this processing technique in that the level of the scattered field associated with the taped hole was unexpected.

The calculated patterns simulated by the OSU Reflector Antenna Code [4,5] were also processed to further verify the locations of the radiation centers since theoretically, one knows exactly where the locations of the radiation centers are for a circular reflector. The calculated far zone H-plane pattern is given in Figure 6. The cross range responses for $\theta_o = 0°$ and $20°$ with $\Delta\theta = 5°$ are shown in Figure 7. The responses calculated from the measured pattern are also shown in the same figure for comparison. It is seen from Figure 7(b) that the contribution from the hole at the vertex does not appear since it was not modeled in the calculation. Also note that the contributions due to the edge diffractions are much stronger in the calculated pattern than

12

(A): MAIN REFLECTOR EDGE
(B): STRUT END POINT
(C): FEED SPILLOVER, SUPPORT STRUCTURE
(D): HOLE
(E): STRUT END POINT
(F): MAIN REFLECTOR EDGE

(a) $\phi=15°$

(A): MAIN REFLECTOR EDGE, STRUT END POINT
(B): FEED SPILLOVER, SUPPORT STRUCTURE
(C): HOLE
(D): STRUT END POINT
(E): MAIN REFLECTOR EDGE, STRUT END POINT

(b) $\phi=30°$

Figure 5.   Cross range response of the measured off-principal patterns for the 8′ prime focus fed reflector at $\theta_o=20°$, $\Delta\theta=5°$.

13
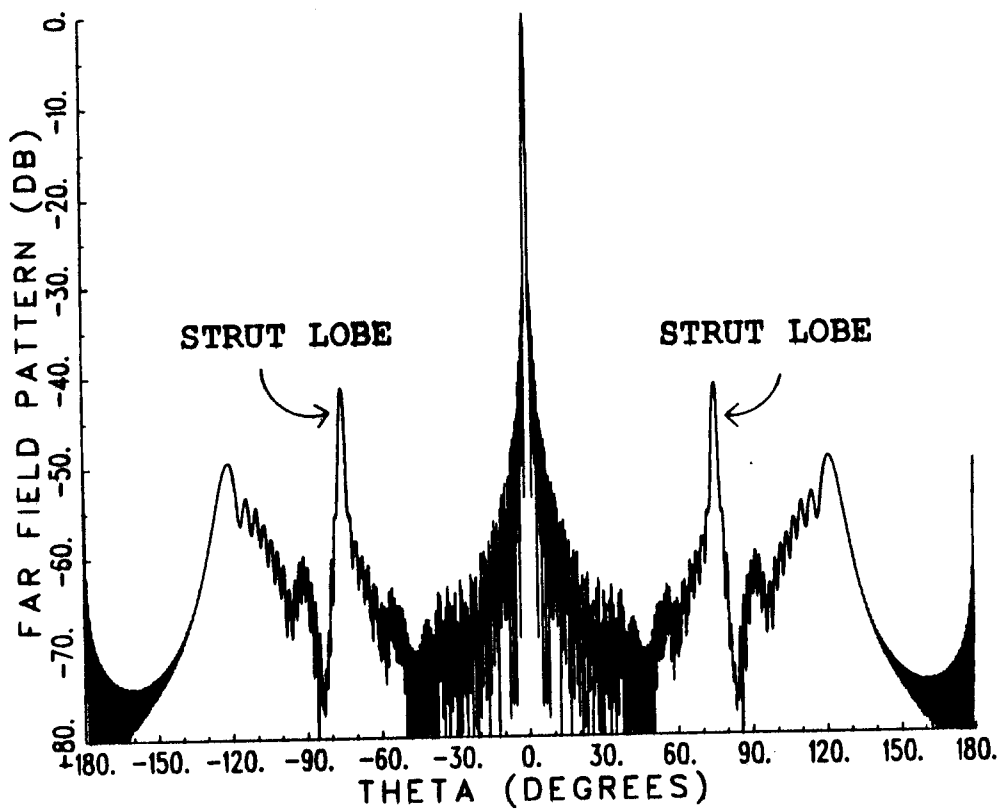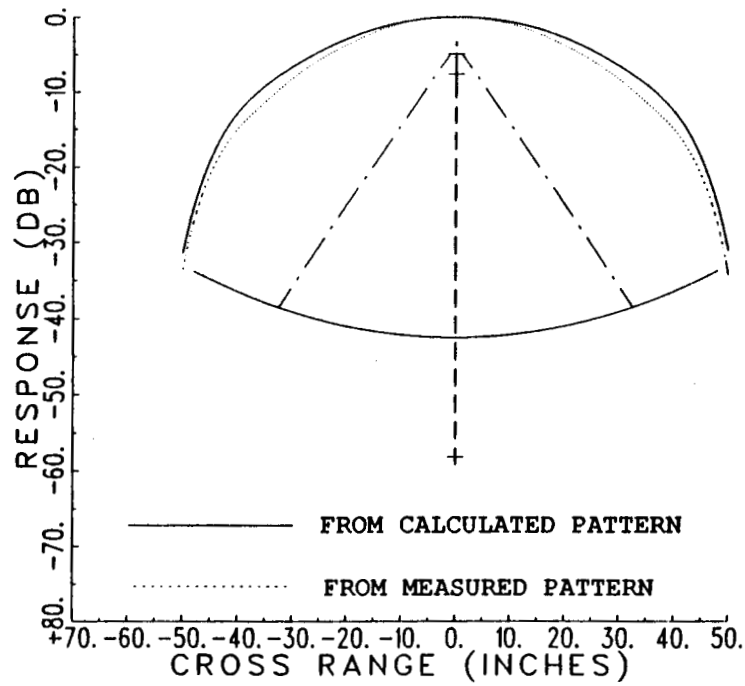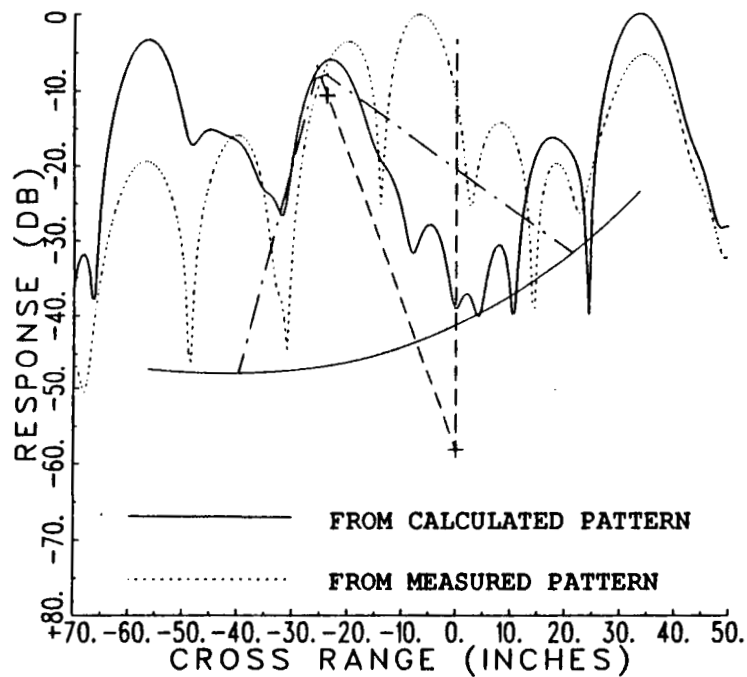
Figure 6. H-plane pattern of the 8′ prime focus fed reflector
calculated by the OSU Reflector Antenna Code.

14

(a) $\theta_o = 0°$, $\Delta\theta = 5°$

(b) $\theta_o = 20°$, $\Delta\theta = 5°$

Figure 7.   Cross range response of the calculated H-plane patterns for the 8' prime focus fed reflector.

15

in the measured one. This is because the real reflector had a rolled edge; whereas, a knife edge was assumed in the simulation. It is also noted that the cross range response for $\theta_o = 0°$ describes the distribution of the fields across the reflector aperture on the pattern plane. This distribution is similar to the YSUM distribution [5,6] used by the OSU Reflector Antenna Code to improve the computation efficiency of the far zone aperture integration solution. The YSUM's are actually the summation of aperture fields along the lines perpendicular to the pattern plane. The YSUM distribution calculated by the Reflector Antenna Code is shown in Figure 8 for comparison. The difference between the YSUM distribution and the cross range response is that only the aperture fields are included in the YSUM's; whereas in the cross range response, the scattered fields from the feed support structure and feed spillover are also included. The cross range responses of the calculated edge diffracted fields, aperture blockage, strut scattered fields and feed spillover are given in Figure 9 for $\phi = 0°$ and $\theta_o = 20°$. Note that the cross range processing clearly identifies the location of each radiation center properly and indicates a relative radiation level which makes it most appropriate for diagnostic purposes.

These examples illustrate other very useful applications for this processing. If one has a simulation of the antenna design, he can process his simulation data and compare the results with measured ones. The difference in the radiation center levels indicates improper radiation levels in the calculation; whereas, the lack of radiation centers in the model means that the simulation was not complete. Note

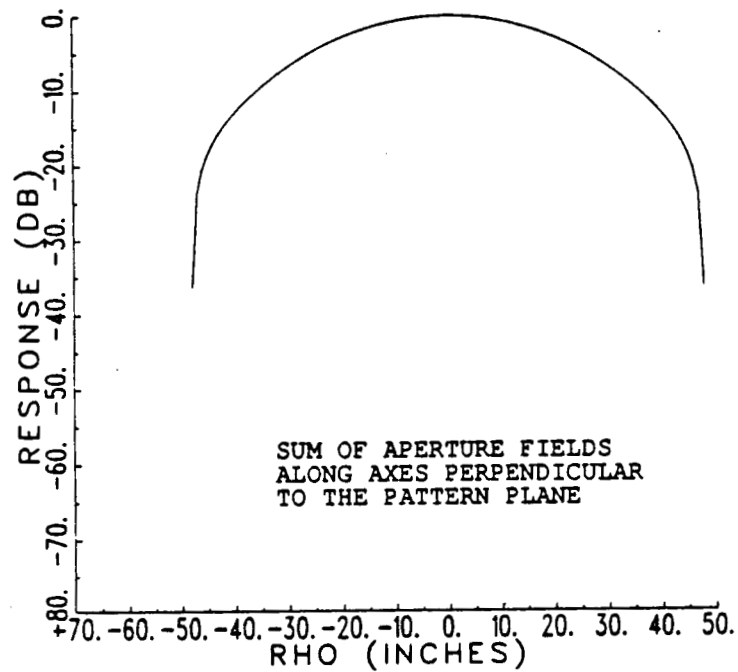16

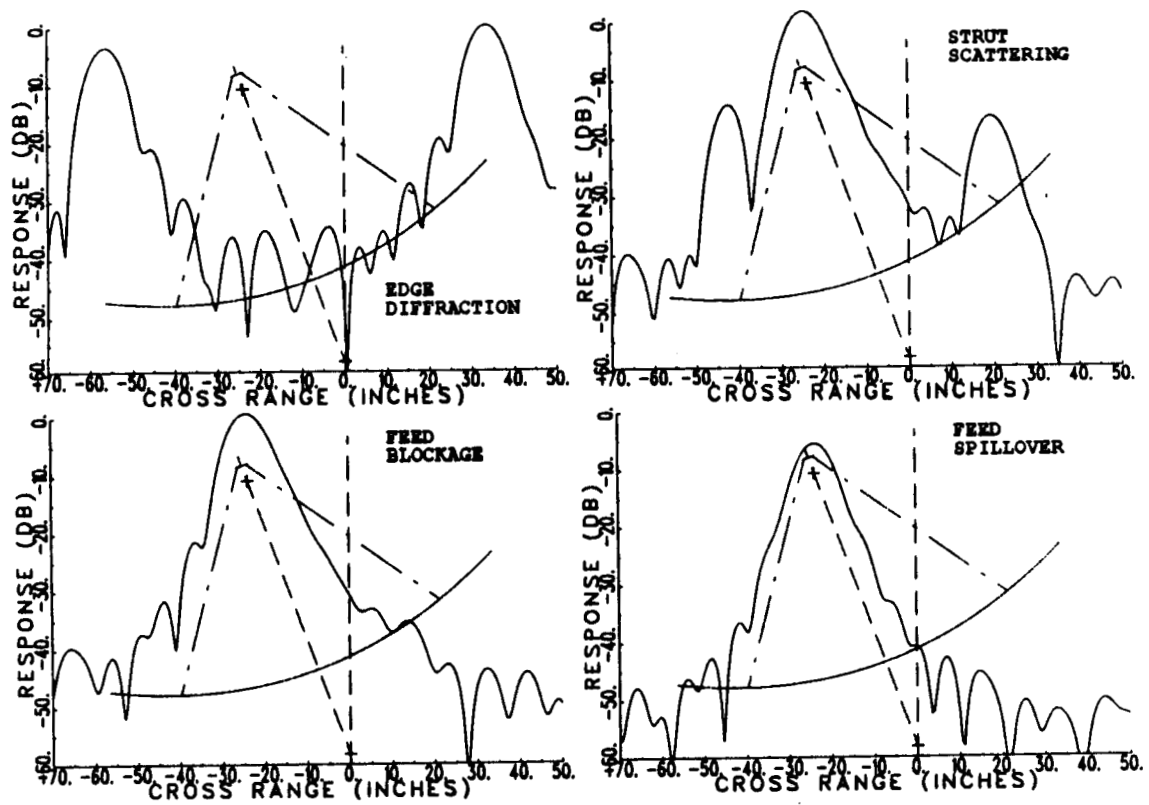Figure 8.   Calculated H-plane YSUM distribution of the 8′ prime focus
fed reflector.

Figure 9. Cross range responses of the different contributions to the
calculated H-plane pattern at $\theta_o=20°$ of the 8' prime focus
fed reflector.

18

that the lack of radiation centers can also indicate measurement errors in that certain centers can be associated with range problems, for example.

B. 8' Cassegrain Antenna System

In this section, the results of cross range processing of the patterns of an 8' Cassegrain reflector are presented. The geometry of this reflector is shown in Figure 10(a). The focal length of the main reflector was 35.8" and the distance between the two focii of the subreflector was 22.262". The measured H-plane pattern at 11.0 GHz for this antenna with a conical horn feed is shown in Figure 10(b). The cross range responses of the H-plane patterns at $\theta_o=0°$ and 30° with $\Delta\theta=5°$ are given in Figure 11. The H-plane pattern calculated by the Reflector Code is shown in Figure 12 with the cross range responses at $\theta_o=0°$ and 30° shown in Figure 13. Note that the center of rotation was 21.6" behind the vertex of the reflector for this case. From the response for $\theta_o=0°$, one can see the significant blockage effects caused by the subreflector on the aperture distribution. One can also easily identify the various radiation centers from the response for $\theta_o=30°$. It is also obvious that the direct spillover from the primary feed is very strong compared to the other contributions.

It is very interesting to note that in the prime focus fed reflector pattern, there were two very significant strut lobes which occur at $\theta \sim \pm 75°$ as shown in Figures 3(b) and 6; however, these two lobes did not appear in the pattern of the Cassegrain reflector as shown in

19
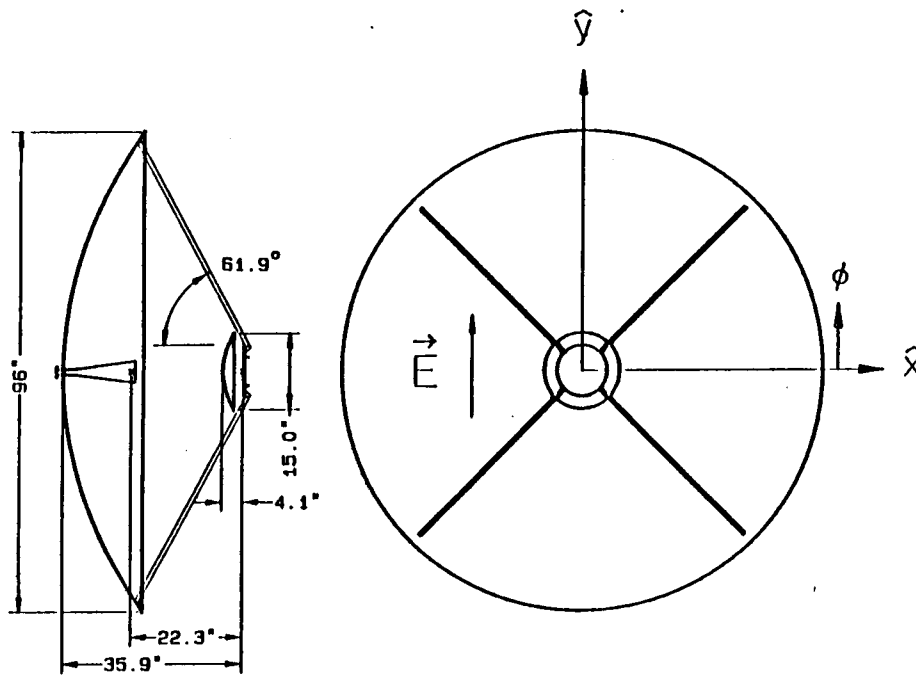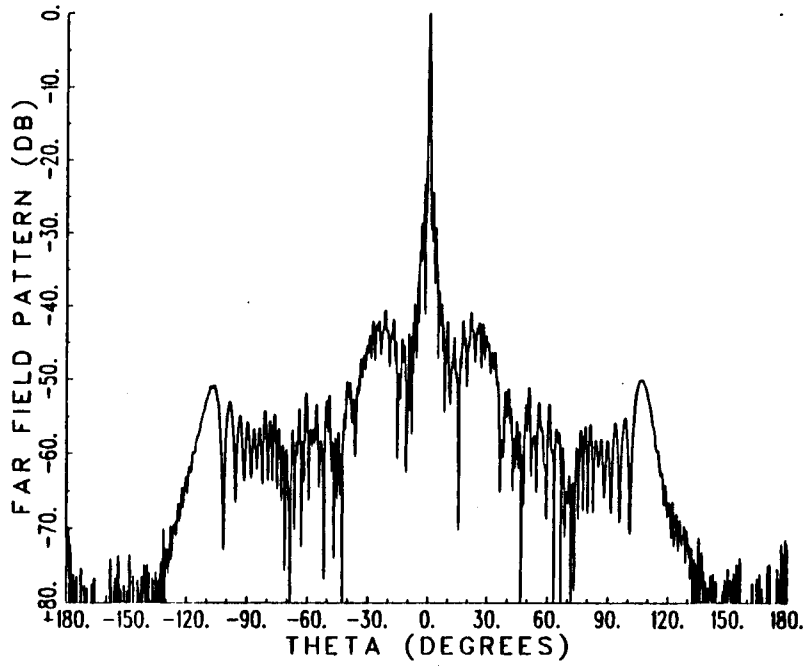
(a) Geometry

(b) Measured H-plane pattern

Figure 10. Geometry and measured H-plane pattern of an 8' Cassegrain reflector.

20

(a) $\theta_o=0°$, $\Delta\theta=5°$

(A) : MAIN REFLECTOR EDGE
(B) : STRUT END POINT
(C) : SUBREFLECTOR EDGE
(D) : FEED SPILLOVER, SUBREFLECTOR EDGE
(E) : STRUT END POINT
(F) : MAIN REFLECTOR EDGE

(b) $\theta_o=30°$, $\Delta\theta=5°$
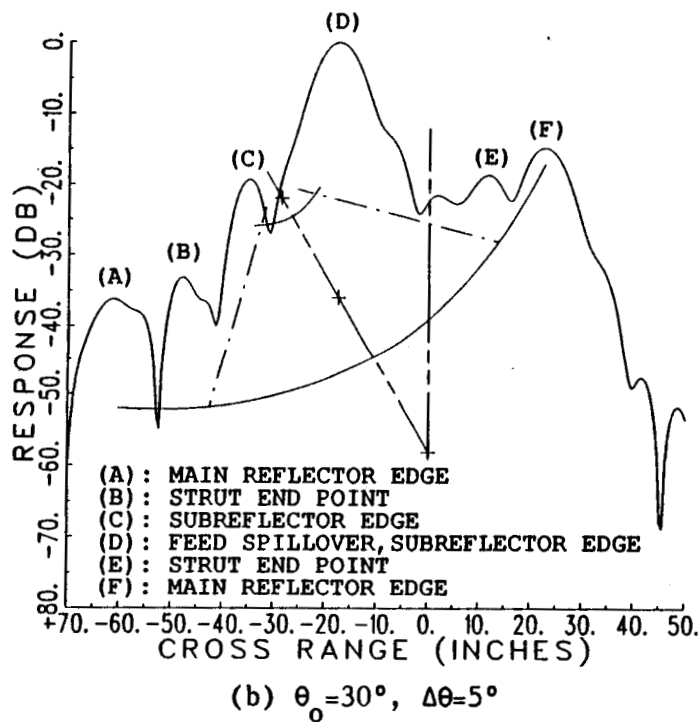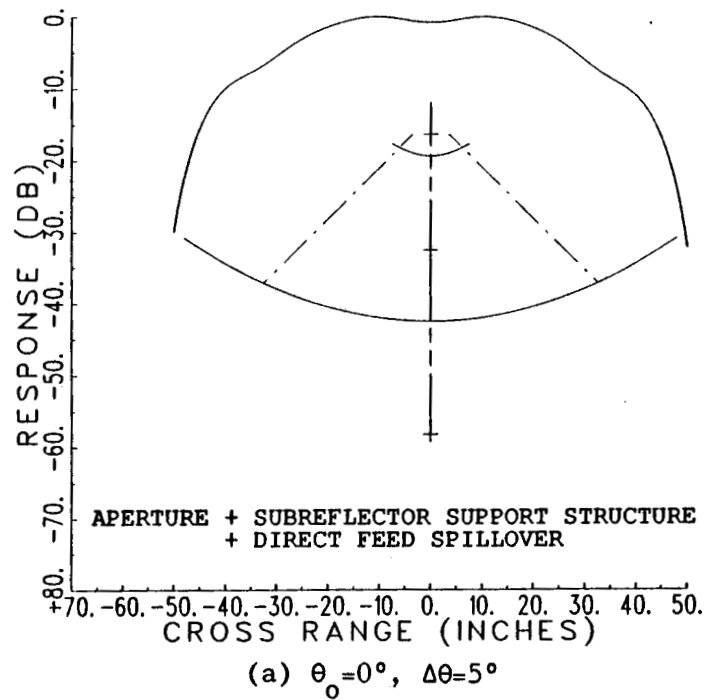
Figure 11. Cross range response of the measured H-plane pattern for the 8' Cassegrain reflector.

21
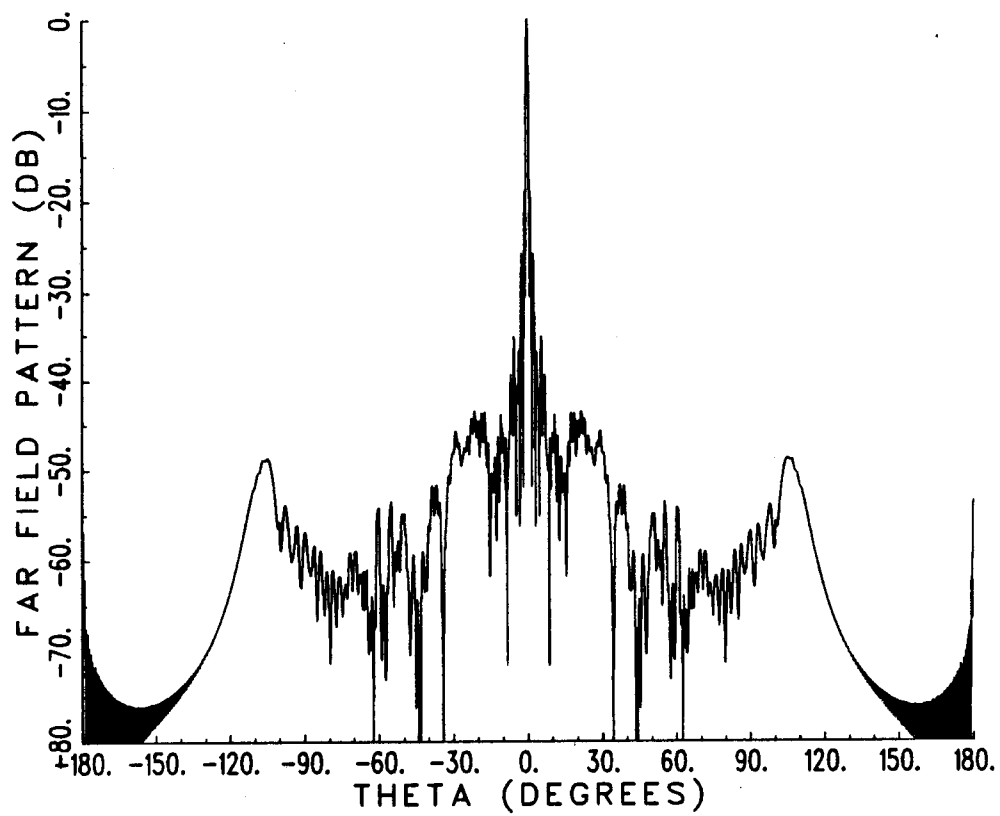
Figure 12. H-plane pattern of the 8' Cassegrain reflector calculated by the OSU Reflector Antenna Code.

22

(a) $\theta_o = 0°$, $\Delta\theta = 5°$

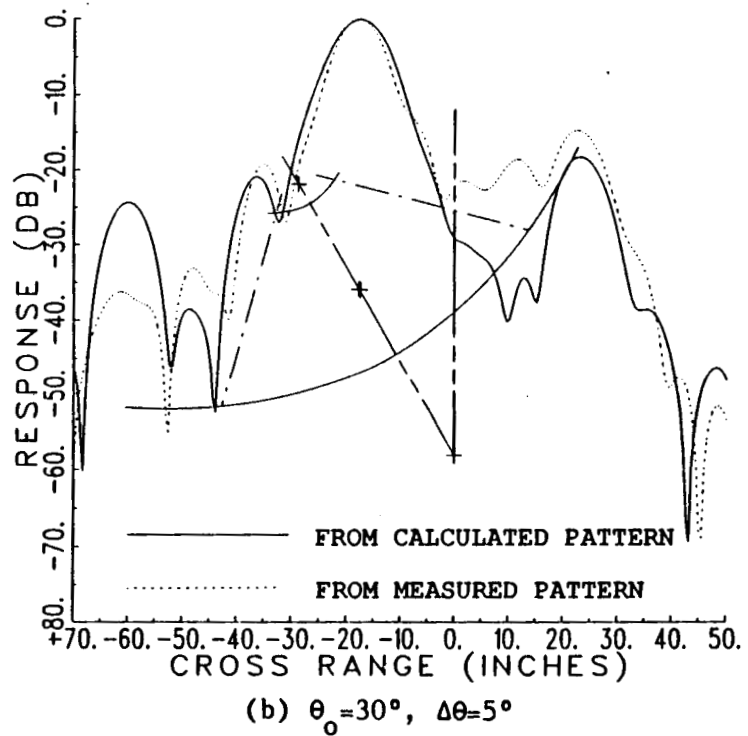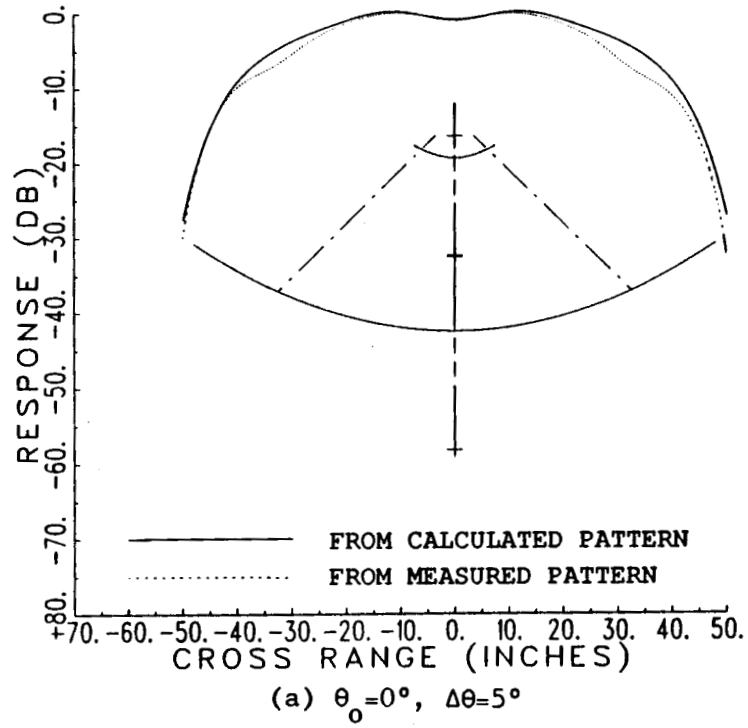(b) $\theta_o = 30°$, $\Delta\theta = 5°$

Figure 13. Cross range response of the calculated H-plane pattern for the 8' Cassegrain reflector.
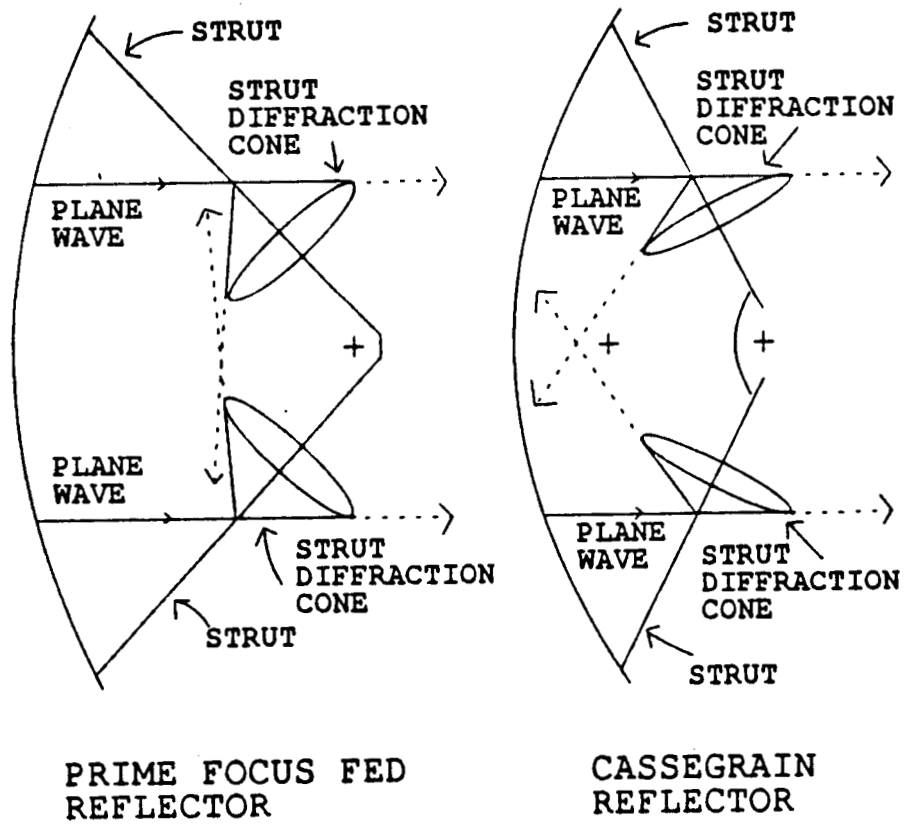
Figure 14. Illustration of scattering by struts.

Figures 10(b) and 12. These strut lobes were caused by the scattering from struts with plane wave incidence which is the reflected field from the main reflector. The strut scattered field is most significant along certain directions which lie on a diffraction cone [7,8] as illustrated in Figure 14. The half angle of the cone depends on the angle of the strut with respect to the axis of the reflector. In the 8' Cassegrain reflector, the half angle of the strut diffraction cone is larger than the one in the prime focus fed reflector as shown in Figure 14. Consequently, the strut scattered fields at the wide angles from the reflector axis were blocked by the main reflector surface and then scattered in other directions. Thus, the cross range response for the Cassegrain reflector pattern indicates the secondary scattering from the struts.

In order to evaluate this strut scattering for the Cassegrain case, let us consider the $\phi=45°$ measured pattern in that one can easily trace the rays reflected by the struts in this pattern plane. The cross range response for $\theta_o=30°$ in the $\phi=45°$ plane is shown in Figure 15 with the dashed line tracing the ray: feed $\rightarrow$ subreflector $\rightarrow$ main reflector $\rightarrow$ strut $\rightarrow$ main reflector $\rightarrow$ far zone. This contribution is normally not simulated in any computer code, although the cross range response shows that it is a very important term.

IV. CONCLUSIONS

A diagnostic technique to obtain cross range radiation centers based on antenna radiation patterns has been presented in this report. This method is similar to the synthetic aperture processing of scattered

25

(A): MAIN REFLECTOR EDGE,STRUT END POINT
(B): SUBREFLECTOR EDGE
(C): FEED SPILLOVER,SUBREFLECTOR EDGE
(D): FEED-SUBREFLECTOR-MAIN REFLECTOR
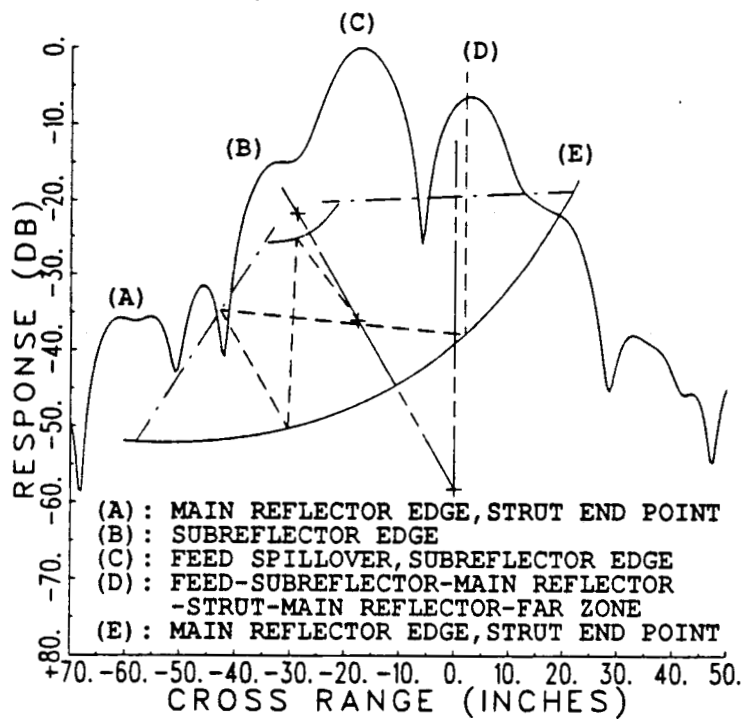   -STRUT-MAIN REFLECTOR-FAR ZONE
(E): MAIN REFLECTOR EDGE,STRUT END POINT

Figure 15. Cross range response of the measured 45° plane pattern for the 8' Cassegrain reflector with $\theta_o = 30°$ and $\Delta\theta = 5°$.

26

fields in the radar application. Coherent processing is used to determine various radiation centers based on far zone pattern data provided that adjacent centers are separated far enough so that their locations can be resolved. Although one can also increase the angular boundary of integration for $I(\gamma)$ to improve the resolution, this is restricted by the assumption that $\cos\psi \approx 1$ and $\sin\psi \approx \psi$ in the derivation of $I(\gamma)$. Cross range processing results based on the far-zone patterns associated with two 8' reflector antennas were presented to illustrate as well as validate this concept.

This technique can be used to diagnose the radiation properties of an antenna and/or evaluate its radiation centers versus those used in the design of the antenna system. In this regard, it is used to indicate the unexpected radiation centers such as the hole scattering identified in our example. On the other hand, it can provide information about contributions from the antenna which are not modeled in a numerical simulation, such as the strut scattered fields which reflect from the main reflector surface in the 8' Cassegrain reflector case. Although this technique only provides cross range information, one can scan the antenna in the θ and ϕ directions to obtain a two-dimensional image such as used by the holographic community, or scan the antenna in frequency to obtain so-called "down-range" radiation center information.

Now that an antenna engineer can very easily and accurately measure phase, all these diagnostic processing tools are at his finger tips. Once the value of these methods become more widespread in the antenna community, it is expected that improved designs will result because one

can better evaluate pattern performance in terms of the individual

mechanisms that create the resulting pattern. With this in mind, this

report has not attempted to examine all the ways that this type of

processing can be used for antenna applications but rather to illustrate

their general value and strongly suggest that they be used in future

antenna designs.

REFERENCES

[1] D.L. Mensa, High Resolution Radar Imaging, Artech House, Inc.,
    1981.

[2] J.C. Bennett, A.P. Anderson, P.A. McInnes, and A.J.T. Whitaker,
    "Microwave Holographic Metrology of Large Reflector Antennas," IEEE
    Trans. on Antennas and Propagation, Vol. AP-24, No. 3, pp. 295-303,
    May 1976.

[3] Y. Rahmat-Samii, "Surface Diagnosis of Large Reflector Antennas
    Using Microwave Holographic Metrology — An Iterative Approach,"
    Radio Science, Vol. 13, pp. 1205-1217, September-October 1984.

[4] R.C. Rudduck and Y.C. Chang, "Numerical Electromagnetic Code —
    Reflector Antenna Code NEC-REF (Version 2) Part I: User's Manual,"
    The Ohio State University ElectroScience Laboratory Technical
    Report 712242-16, generated under Contract N00123-79-C-1469 for
    Naval Regional Contracting Office, Long Beach, California 90822,
    December 1982.

[5] Y.C. Chang and R.C. Rudduck, "Numerical Electromagnetic Code —
    Reflector Antenna Code NEC-REF (Version 2) Part II: Code Manual,"
    The Ohio State University ElectroScience Laboratory Technical
    Report 712242-17, generated under Contract N00123-79-C-1469 for
    Naval Regional Contracting Office, Long Beach, California 90822,
    December 1982.

[6] S.H. Lee and R.C. Rudduck, "Aperture Integration and GTD Techniques
    Used in the NEC Reflector Antenna Code," IEEE Trans. on Antennas
    and Propagation, Vol. AP-33, No. 2, pp. 189-194, February 1985.

[7] S.H. Lee, R.C. Rudduck, C.A. Klein and R.G. Kouyoumjian, "A GTD
    Analysis of the Circular Reflector Antenna Including Feed and Strut
    Scatter," The Ohio State University ElectroScience Laboratory
    Report 4381-1, generated under contract F30602-76-C-0024 with Rome
    Air Development Center, May 1977.

[8] W.V.T. Rusch, O Sorensen and J.W.M. Baars, "Radiation Cones from
    Feed-Support Struts of Symmetric Paraboloidal Antennas," IEEE
    Trans. on Antennas and Propagation, Vol. AP-30, pp. 786-790, July
    1982.

50272-101

REPORT DOCUMENTATION PAGE	1. REPORT NO.	2.	3. Recipient's Accession No.

4. Title and Subtitle	5. Report Date
A DIAGNOSTIC TECHNIQUE USED TO OBTAIN CROSS RANGE RADIATION CENTERS FROM ANTENNA PATTERNS	May 1988
	6.

7. Author(s)	8. Performing Organization Rept. No.
T.H. Lee and W.D. Burnside	716148-30

9. Performing Organization Name and Address	10. Project/Task/Work Unit No.
The Ohio State University ElectroScience Laboratory 1320 Kinnear Road Columbus, Ohio 43212	11. Contract(C) or Grant(G) No. (C) (G) NSG-1613

12. Sponsoring Organization Name and Address	13. Type of Report & Period Covered
National Aeronautics and Space Administration Langley Research Center Hampton, Virginia 23665	Technical
	14.

15. Supplementary Notes

16. Abstract (Limit: 200 words)

A diagnostic technique to obtain cross range radiation centers based on antenna radiation patterns is presented in this report. This method is similar to the synthetic aperture processing of scattered fields in the radar application. Coherent processing of the radiated fields is used to determine the various radiation centers associated with the far-zone pattern of an antenna for a given radiation direction. This technique can be used to identify an unexpected radiation center that creates an undesired effect in a pattern; on the other hand, it can improve a numerical simulation of the pattern by identifying other significant mechanisms. Cross range results for two 8' reflector antennas are presented to illustrate as well as validate this technique.

17. Document Analysis   a. Descriptors

b. Identifiers/Open-Ended Terms

c. COSATI Field/Group

18. Availability Statement	19. Security Class (This Report)	21. No. of Pages
	Unclassified	28
	20. Security Class (This Page)	22. Price
	Unclassified	

(See ANSI–Z39.18)   See Instructions on Reverse   OPTIONAL FORM 272 (4–77)
(Formerly NTIS–35)
Department of Commerce